Published in final edited form as:
J Mol Biol. 2010 March 12; 396(5): 1211–1226. doi:10.1016/j.jmb.2009.12.060.

An extracellular disulfide bond forming protein (DsbF) from *Mycobacterium tuberculosis*: Structural, biochemical and gene expression analysis

Nicholas Chim[1], **Robert Riley**[3], **Juliana The**[4], **Soyeon Im**[4], **Brent Segelke**[5], **Tim Lekin**[5], **Minmin Yu**[6], **Li Wei Hung**[7], **Tom Terwilliger**[8], **Julian P. Whitelegge**[9,10], and **Celia W. Goulding**[1,2,*]

[1]Department of Molecular Biology and Biochemistry, UCI, Irvine, CA 92697

[2]Department of Pharmaceutical Sciences, UCI, Irvine, CA 92697

[3]Department of Human Genetics, David Geffen School of Medicine, UCLA, Los Angeles, CA 90095

[4]UCLA-DOE Institute of Genomics and Proteomics, P.O. Box 951570, Los Angeles, CA 90095-1570

[5]Biology and Biotechnology Program, Lawrence Livermore National Laboratory, Livermore, CA 94551

[6]Physical Biosciences Division, Lawrence Berkeley National Laboratory, Berkeley, CA 94720

[7]Physics Division, Los Alamos National Laboratory, Los Alamos, NM, 87545

[8]Biosciences Division, Los Alamos National Laboratory, Los Alamos, NM, 87545

[9]Department of Chemistry and Biochemistry, UCLA, Los Angeles, CA 90095-1570

[10]The Pasarow Mass Spectrometry Laboratory, NPI-Semel Institute, David Geffen School of Medicine, UCLA, Los Angeles, CA 90095

Abstract

Disulfide bond forming (Dsb) proteins ensure correct folding and disulfide bond formation of secreted proteins. Previously, we showed that *Mycobacterium tuberculosis* DsbE (*Mtb* DsbE, Rv2878c) aids *in vitro* oxidative folding of proteins. Here we present structural, biochemical and gene expression analyses of another putative *Mtb* secreted disulfide bond isomerase protein homologous to *Mtb* DsbE, *Mtb* DsbF (Rv1677). The X-ray crystal structure of *Mtb* DsbF reveals a conserved thioredoxin fold although the active-site cysteines may be modeled in both oxidized and reduced forms, in contrast to the solely reduced form in *Mtb* DsbE. Furthermore, the shorter loop region in *Mtb* DsbF results in a more solvent-exposed active site. Biochemical analyses show that, similar to *Mtb* DsbE, *Mtb* DsbF can oxidatively refold reduced, unfolded hirudin and has a comparable pK_a for the active-site solvent-exposed cysteine. However, contrary to *Mtb* DsbE, the *Mtb* DsbF redox potential is more oxidizing and its reduced state is more stable. From computational

*Address correspondence to: Celia Goulding, celia.goulding@uci.edu, Phone: (949) 824 0337, Fax: (949) 824 8551.

Protein Data Bank accession number

The atomic coordinates and structure factors for the crystal structure of *Mtb* DsbF modeled with its active-site cysteines in both their reduced and oxidized states have been deposited with the Protein Data Bank (RCSB, http://www.rcsb.org/pdb) as entry 3IOS.

genomics analysis of the *M. tuberculosis* genome, we identified a potential *Mtb* DsbF interaction partner, Rv1676, a predicted peroxiredoxin. Complex formation is supported by protein co-expression studies and inferred by gene expression profiles, whereby *Mtb* DsbF and Rv1676 are upregulated under similar environments. Additionally, comparison of *Mtb* DsbF and *Mtb* DsbE gene expression data indicate anticorrelated gene expression patterns, suggesting that these two proteins and their functionally linked partners constitute analogous pathways that may function under different conditions.

Keywords

Mycobacterium tuberculosis; disulfide bond forming protein; structure-function; gene expression data; X-ray crystallography

Introduction

Most disulfide oxidoreductase proteins contain a conserved thioredoxin-like domain and share a common sequence motif (CxxC) at their active sites. These ubiquitous proteins have a variety of mechanistic roles including protein folding, electron transport and bioenergetics in all three kingdoms of life. The family of disulfide oxidoreductase proteins include thioredoxin, eukaryotic protein disulfide bond isomerase, glutaredoxin [1], peroxiredoxin [2] and disulfide bond forming (Dsb) proteins.

Dsb proteins are best characterized in *Escherichia coli*. These proteins reside in the periplasmic space of gram-negative bacteria and are necessary for correct folding of many cell envelope proteins [3]. Over the last decade, Dsb proteins, and in particularly DsbA, have been shown to be involved in virulence in toxin-secreting gram-negative bacteria such as *E. coli* [4], *Yersinia pestis* [5], *Shigella sp*. [6] and *Vibrio cholerae* [7; 8]. *E. coli* DsbA is a monomer that catalyses the oxidation of reduced, unfolded proteins [9; 10]. DsbA is reoxidized by the transmembrane protein DsbB, which is in turn oxidized by components of the electron transport pathway [11; 12]. Another well-characterized Dsb protein is *E. coli* DsbE, a monomeric thioredoxin-like protein involved in cytochrome c maturation [13]. DsbE has been implicated in the reduction of thiol ether linkers to apocytochrome c prior to heme ligation by CcmF and CcmH [13; 14; 15]. *E. coli* DsbD is a transmembrane protein spanning the cytoplasmic membrane responsible for maintaining DsbE in its reduced state [16]. Finally, *E. coli* DsbC and DsbG are homodimers with disulfide bond isomerase activity, which are also maintained in their reduced state by the transmembrane protein DsbD [17].

In *Mycobacterium tuberculosis* (*M. tuberculosis*), the only Dsb proteins identified to-date are *Mtb* DsbE (Rv2878c aka MPT53) [18], its homolog annotated as *Mtb* DsbF (Rv1677) and its potential redox, transmembrane protein partner *Mtb* DsbD (Rv2874) [19]. The presence of Dsb proteins in *M. tuberculosis* suggest these proteins are necessary for the correct folding of disulfide bond rich cell-wall associated, potential periplasmic [20] and secreted extracellular proteins. Within the *M. tuberculosis* proteome, it has been predicted that over 160 proteins are secreted, of which 60% may contain disulfide bonds based on their cysteine content, implying that disulfide bond forming proteins are required for correct folding of approximately 90 secreted proteins [18]. *M. tuberculosis* secreted proteins have many different roles including involvement in virulence, pathogenicity and cell-wall maintenance; thus, interruption of their folding pathways may prevent mycobacterial infectivity and viability. As *M. tuberculosis* is a pathogenic bacterium responsible for tuberculosis (TB), which causes approximately 2 million deaths and 8 million new cases per year, [21; 22], the study of Dsb protein systems in *M. tuberculosis* may offer new insight into its virulence and provide novel anti-TB drug targets [23; 24].

Recently, we biochemically and structurally characterized a homolog of *E. coli* DsbE, a secreted protein, *Mtb* DsbE (Rv2878c) [18]. We determined the crystal structure of *Mtb* DsbE to 1.1 Å resolution, which revealed a thioredoxin-like domain with a typical CxxC active site. The active-site cysteines in the structure of *Mtb* DsbE are in their reduced state. Additionally, the pK_a of the active-site, solvent-exposed cysteine was determined to be approximately 2 units lower than that of gram-negative DsbE homologs. Finally, the reduced form of *Mtb* DsbE is more stable than the oxidized form, and *Mtb* DsbE is able to oxidatively refold leech hirudin. Structural and biochemical analyses imply that *Mtb* DsbE functions as a thiol oxidase, unlike gram-negative bacteria DsbE proteins that have been shown to be weak reductases [25]. On the contrary, *Mtb* DsbE is functionally analogous to *E. coli* DsbA, folding and ensuring correct disulfide bond formation in secreted proteins, although structurally *E. coli* DsbA has an additional domain that caps the thioredoxin-like active site [26].

In this study, we have determined the 1.6 Å resolution structure of *Mtb* DsbF (Rv1677), a predicted extracellular disulfide bond forming protein homologous to *Mtb* DsbE. The active-site cysteines of *Mtb* DsbF are in both their oxidized and reduced forms. Further characterization reveals that *Mtb* DsbF has a redox potential of -87 mV comparable to that of *E. coli* DsbA (-89 to -119 mV) [27; 28], which is confirmed by its ability to refold hirudin. Additionally, we show that *Mtb* DsbF forms a potential transient protein complex with its genomic neighbor Rv1676, a predicted peroxiredoxin, and that these two proteins have correlated gene expression profiles suggesting that they may potentially function in the same biochemical pathway. Both *Mtb* DsbF and *Mtb* DsbE appear to be part of larger groups of coexpressed genes, suggesting the possible involvement of *Mtb* DsbE and *Mtb* DsbF in complexes or pathways. We show that the expression profiles of both *Mtb* DsbF and Rv1676 are inversely correlated with respect to *Mtb* DsbE, suggesting that they, and in turn their coexpressed partners, are induced under different conditions. Finally, we consider the environmental conditions under which *Mtb* DsbF and its protein partners may be expressed.

Results

The complete sequence and subsequent annotation of the *M. tuberculosis* genome has allowed the prediction of many genes and gene functions by homology. Rv2878c and Rv1677 were annotated as putative secreted disulfide bond forming proteins DsbE and DsbF, respectively [29]. A recent study of *Mtb* DsbE showed that this protein was biochemically more similar to *E. coli* DsbA rather than to *E. coli* DsbE [18]. This result led to the investigation of the structure, biochemistry and gene expression patterns of *Mtb* DsbF in an attempt to determine the function of *Mtb* DsbF and the pathway in which it may function.

Structural Overview of *Mtb* DsbF

The crystal structure of the mature form of *Mtb* DsbF (without its signal peptide, residues 1-38, which was predicted to high significance by SignalP [30]) consists of a thioredoxin fold, with its distinct structural motif consisting of a four-stranded β-sheet made up of β3, β4, β6 and β7 and three flanking α-helices corresponding to α3, α5 and α6 (Figure 1a). As in the structure of *Mtb* DsbE [18], a long α-helix (α4) and a β-strand (β5) (forming a five-stranded β-sheet) are found after the β3-α3-β4 motif of the thioredoxin fold. At the N-terminus of the structure there is an additional smaller domain, which consists of a short 3_{10}-helix (α1), two β-strands (β1 and β2) and another short 3_{10}-helix (α2). The cysteines adopt a right-handed hook conformation at the N-terminus of helix α3 as found for most active-site cysteines in the thioredoxin superfamily fold. The electron density for the two active-site cysteines, Cys81 and Cys84, is most consistent with a model in which conformations of the oxidized and reduced forms of the cysteines are observed, hence we modeled both the oxidized and reduced forms into the structure. The conformation in which the cysteines are oxidized has a distance of 2.06 ± 0.20

Å between the two Sγ atoms (Figure 1b), which is consistent with other observed disulfide bonds [31]. Only the Sγ atom of Cys81 in the dithiol is exposed on the protein surface, while Sγ of Cys84 is buried. The sulfur atom of Cys81 is stabilized by weak hydrogen bonds to the amide N atom of Thr83 (3.33 Å) and the Oε1 atom of Gln146 (4.05 Å); the Sγ atom of Cys84 is hydrogen bonded to the carbonyl O atom of Ala78 (4.00 Å) and to a water molecule (3.80 Å) which is in turn hydrogen-bonded to Oε1 of Glu87 (2.59 Å) and Nε1 of Trp75 (2.50 Å). Both Cys81 and Cys84 have a hydrophobic interaction with conserved *cis*-Pro147 (4.42 Å and 4.80 Å respectively). Interestingly, the reduced form also appears to be present within the crystal structure with occupancy of approximately 50% (Figure 1c). The distance between the active-site cysteines modeled in the reduced form conformation for *Mtb* DsbF is 3.69 ± 0.10 Å. The sulfur atom of Cys81 is stabilized by hydrogen bonds to the amide N atom of Thr83 (3.78 Å) and the Oε1 atom of Gln146 (3.30 Å); the Sγ atom of Cys84 is hydrogen bonded to the carbonyl O atom of Ala78 (3.78 Å) and to a water molecule (3.45 Å) which is in turn hydrogen-bonded to Glu87 and Trp75 as described for the oxidized conformation.

Determination of the Redox Potential of *Mtb* DsbF and comparison with *Mtb* DsbE

To further characterize *Mtb* DsbF, the redox potential relative to that of glutathione was determined. This redox potential compares the ability of reduced glutathione to transfer electrons to a protein. The K_{eq} of *Mtb* DsbF is ~40 ± 5 μM (Figure 2a). The corresponding standard redox potential (E'_0) calculated for *Mtb* DsbF is −89 ± 9 mV. In comparison with the standard redox potential of two thiol oxidases, *Mtb* DsbE (−128 mV) [18] and *E. coli* DsbA (between −89 to −119 mV) [27; 28], and reductase *E. coli* thioredoxin (−269 mV) [32], the standard redox potential of *Mtb* DsbF suggests that it is also a thiol oxidase which has stronger oxidizing potential than its homolog *Mtb* DsbE.

Analysis of oxidase activity of *Mtb* DsbF by mass spectrometry

Reduced, unfolded hirudin from *Hirudo medicinalis* was used to assess the oxidative protein folding ability of *Mtb* DsbF. Hirudin is an inhibitor of thrombin and contains three intramolecular disulfide bridges. Mass spectrometry analysis of commercial native hirudin revealed, besides significant impurities, a major peak (*m/z* 6765) followed by several smaller peaks ranging up to *m/z* 7088, which is consistent with previous reports that hirudin is a non-homogenous protein that contains several variants [33]. Reverse-phase HPLC was used to enhance the homogeneity of the *m/z* 6765 peak, as well as to remove contaminating proteins. The resulting mass spectrometry data for HPLC-purified hirudin indicated that the *m/z* 6765 peak was the predominant peak. The corresponding peaks for reduced, unfolded hirudin showed a uniform *m/z* increase of 6 Da. Furthermore, the addition of iodoacetamide to reduced, unfolded hirudin carbamidomethylated the free cysteines as observed by the mass increase of six 57 Da increments (+342 Da mass). The predominant peak was thus chosen to monitor the regeneration of reduced, unfolded hirudin (5 pmol) to the fully oxidized native state in the absence and presence of stoichiometric quantities of *Mtb* DsbF (5 pmol). At various time points, the reactions were quenched by the addition of iodoacetamide and analyzed by mass spectrometry. In the absence of *Mtb* DsbF, a small quantity of native hirudin was observed after 8 hrs (Figure 2b), presumably due to spontaneous, air-mediated oxidation as previously reported [18]. However, when reduced, unfolded hirudin was incubated with *Mtb* DsbF, mass spectrometry data showed new peaks at the zero time point corresponding to the immediate quenching of the free thiols by the covalent modification with iodoacetamide molecules (57 Da increments), which decrease over the 8 hr reaction period. Conversely, the native hirudin peak increases over the same time period, suggesting that *Mtb* DsbF is capable of oxidizing substrate proteins, and is comparable to the oxidase activity of *Mtb* DsbE (data not shown), whereby at 8 hours greater than 70% of hiridin is oxidatively refolded (Figure 2b). Significantly, these data concur with the oxidase activity of *E. coli* DsbA, although 100% oxidation occurs after 8 hrs (Figure 2b). Additionally, when incubated with a known reductase,

E. coli thioredoxin (negative control), only a small fraction of oxidized hirudin appears after 8 hrs, as seen for spontaneous air-mediated oxidation of hirudin (Figure 2b).

Thermodynamic Properties of the Redox Forms

To compare stabilities of the different redox forms of *Mtb* DsbF, guanidine hydrochloride-induced unfolding and refolding (data not shown) of both oxidized and reduced forms were examined by circular dichroism. The reduced form of *Mtb* DsbF is more stable than that of the oxidized form, given that the reduced form of the protein denatures at a higher concentration of guanidine hydrochloride compared to the oxidized form (Figure 2c). Calculation of the free energy change ($\Delta\Delta G_{redox}$) between the reduced and oxidized form of *Mtb* DsbF suggests that the reduced form is 24 ± 5 kJ/mol more stable than the oxidized form. This is consistent with the trend observed for *Mtb* DsbE, although the reduced form of *Mtb* DsbE is only 12.4 ± 4 kJ/mol more stable than the oxidized form [18], suggesting greatly increased stability of the reduced form of *Mtb* DsbF.

Determination of the pK_a (Cys81) of *Mtb* DsbF

As the redox potential and thermodynamic properties of the two *Mtb* Dsb proteins are dissimilar, for completeness, we determined the pK_a of the solvent-exposed active-site cysteine of *Mtb* DsbF, which is associated with the redox potential of a protein. The pK_a value of the *Mtb* DsbF Cys81 was measured by observing the change in absorption of the cysteines at 240 nm over a pH range of pH 2-9 (Figure 2d), and was determined to be 5.6 ± 0.3 which is similar to that of *Mtb* DsbE of 5.35 ± 0.2 [18]. Furthermore, the pK_a of Cys81 is relatively acidic compared with the solvent-exposed active-site cysteine of a known reductase, *E. coli* thioredoxin (pK_a of 7.5) [34], although not as acidic as *E. coli* DsbA, which is a known oxidase, where the pK_a of the solvent-exposed active-site cysteine is 3.5 [35].

Potential Protein Interaction Partner for *Mtb* DsbF

Comparative organization across organisms and genomic context within an organism yield information inferring functional linkages between proteins on a genome-wide scale [36; 37]. *M. tuberculosis* genomic organization around the gene *Rv1677* reveals that this gene is in the same operon as *Rv1676*. The final four nucleotides of *Rv1676* contain both the stop-codon for *Rv1676* and the start-codon for *Rv1677* (*Mtb* DsbF). Two bioinformatics methods, gene neighbor and gene cluster, predict with high significance that these two proteins are both transcribed together and may function within a common pathway [38].

To test this hypothesis, *Rv1676* and *Rv1677* were cloned into a single pETDuet double expression vector in which only *Mtb* DsbF encodes a His_6 affinity tag. The cell lysate from the double expression study was then loaded onto a Ni^{2+} charged HiTrap chelating column. After washing all of the non-specifically bound material from the column, the proteins of interest were eluted with an imidazole gradient from 0 – 500 mM (Figure 3a). To verify if *Mtb* DsbF interacts with Rv1676, the fractions from the column elution were run on an SDS-PAGE gel. A small peak from Ni^{2+} affinity chromatography showed both a 15 kDa protein and a second protein with a molecular mass of approximately 24 kDa (Figure 3b, lane 4). After excising and performing in-gel tryptic digestion on these bands, the peptides were eluted from the gel and identified utilizing micro-liquid chromatography with tandem mass spectrometry (μLC-MSMS) (Figure 3b). The results from the in-gel tryptic digestion mass spectrometry experiment showed that the band corresponding to the 24 kDa protein contained peptides from Rv1676. (Figure 3c). Peptides from the 15 kDa band could not be successfully identified as the mass cut-off range within the experiment did not allow for detection of the majority of the peptides from the tryptic digestion of *Mtb* DsbF. However, the 15 kDa protein band migrated identically to *Mtb* DsbF on an SDS-PAGE gel (Figure 3a, lane 3) and MALDI mass spectrometry revealed that molecular mass was consistent with that of *Mtb* DsbF (data not

shown). Under native conditions, Rv1676 when expressed alone is insoluble whereas a small fraction of it is soluble when co-expressed with *Mtb* DsbF. This observation indicates that *Mtb* DsbF is able to maintain some soluble Rv1676, suggesting a potential transient protein complex. Interestingly, Rv1676 has been reported to localize to the mycobacterial membrane or cell-wall vicinity [39], and thus may interact with secreted *Mtb* DsbF. Therefore, *Mtb* DsbF and Rv1676 may function in a common pathway as their genes are contained within the same operon and co-expression studies infer an *in vitro* protein-protein interaction.

Gene Expression Data

To further investigate the experimental data that Rv1676 and *Mtb* DsbF can interact transiently *in vitro*, we looked at the gene expression data from various microarray datasets for *Rv1676* and *Rv1677* compared with its homolog *Rv2878c* (encodes for *Mtb* DsbE), its proposed interaction partners *Rv2874* [18] and predicted membrane protein *Rv2877c* [40]. Gene expression data was extracted and combined from four experimental data sets [41; 42; 43; 44] using a previously documented methodology [45]. Figure 4a demonstrates that the expression of *Rv1676* and *Rv1677* are strongly correlated, which one would predict considering they are located within the same operon. A positive correlation was also observed for the gene expression pattern of *Rv2874*, *Rv2877c* and *Rv2878c*. Thus each group of proteins may represent distinct disulfide bond forming pathways. More interestingly, these two groups of proteins have anticorrelated expression patterns indicating that while one group of Dsb proteins is up-regulated, the other is down-regulated. This implies that the two Dsb groups may be distinct from one another, and are regulated, expressed and function under different environmental conditions in *M. tuberculosis*.

Discussion

Structural Comparison of *Mtb* DsbF and *Mtb* DsbE

Mtb DsbF and *Mtb* DsbE are extremely similar in both sequence and structure but there are two striking differences between their structures. The sequence identity between *Mtb* DsbF and *Mtb* DsbE is 55.4% (Figure 5a), and the crystal structures of *Mtb* DsbF and *Mtb* DsbE can be superimposed with a root mean square derivation of 1.0 Å for 127 C_α atoms. The two structural differences are 1) the active-site cysteines are in different redox states in the crystal form; and 2) one of the loop regions in *Mtb* DsbE is extended compared to *Mtb* DsbF (Figure 5b).

Within the active-site motif CxxC of the *Mtb* DsbF structure, Cys81 and Cys84 are in both oxidized and reduced states whereas in the *Mtb* DsbE structure the active cysteines Cys36 and Cys39 are in their reduced state, 3.69 Å distance between the two Sγ atoms [18] (Figure 5b). The loop between β-strand 7 (β7) and α-helix 6 (α6) is extended by three extra amino acids (inserted in between Arg162 and Gly163 in *Mtb* DsbF) in *Mtb* DsbE compared to *Mtb* DsbF (Figures 5a and 5b). In the *Mtb* DsbE structure, this extended loop ($P^{118}TAA^{121}$) is stabilized due to a hydrophobic interaction with Phe38 within the active-site motif, CPFC (Figure 6a), thus decreasing solvent accessibility of the active site compared to that of *Mtb* DsbF (Figures 6c and 6d, respectively). It should be noted that this loop in the *Mtb* DsbE structure also plays a role in forming a crystallographic homodimeric interface [18]. In contrast, the crystal packing within the *Mtb* DsbF structure reveals no crystallographic dimeric interface. Additionally, within the shorter loop region, NH1 of Arg164 forms a hydrogen bond with the OH group of Thr83 (3.35 Å) within the active-site CPTC motif (Figure 6b), revealing a more solvent-exposed active site compared to that of *Mtb* DsbE (Figures 6d and 6c, respectively).

Structural analyses of the two *Mtb* Dsb proteins along with gram-negative *B. japonicum* DsbE (reductase) and *E. coli* DsbA (oxidase), implicate an amino acid pair that contributes to the

stability of the reduced and oxidized forms of the Dsb proteins. In the reduced form of *Mtb* DsbE, the amino acid pair Trp30 from β-strand 3 (β3) and Glu42 from α-helix 3 (α3) forms a hydrogen bond between Nε1 of Trp30 and Oε1 of Glu42 (2.8 Å), which is flanked by the active-site residues as well as a hydrophobic residue Phe103 from β-strand 4 (β4), Figure 6e. It was proposed previously that this interaction contributes to the stability of the active-site loop to form a conformation where the reduced thiol form is favored [18]. This amino acid (Trp-Glu) pair is conserved throughout mycobacterial and gram-positive DsbE homologs, although these residues in the mixed redox state *Mtb* DsbF structure form a very weak hydrogen bond between Nε1 of Trp75 and Oε1 of Glu87 (4.44 Å) due to the interactions with Tyr142 (Figure 6f) that is superimposable on *Mtb* DsbE Phe103. The OH group of Tyr142 hydrogen bonds to both Nε1 of Trp75 and Oε1 of Glu87 (3.6 and 2.6 Å respectively), preventing a stronger hydrogen bond between Glu87 and Trp75. Additionally, a water molecule hydrogen bonds to all three residues: Nε1 of Trp75 (2.5 Å), OH of Tyr142 (3.8 Å) and Oε1 of Glu87 (2.6 Å), and also to the reduced thiol form of Cys84 (3.5 Å), Figure 6f. In the structures of *Mtb* DsbE, *E. coli* DsbA and *B. japonicum* DsbE, this extensive hydrogen-bonding network is not observed although the hydrogen-bonded amino acid pair across the β-strand and the α-helix is conserved. Additionally, the amino pair in the structure of *E. coli* DsbA, Glu37 and Lys58, is ~0.75 Å closer to each other in the more stable, reduced form compared to the oxidized form [46]. In comparison with *B. japonicum* DsbE [47], the disulfide form is possibly stabilized by the hydrogen bond between Asn86 and Glu98 (3.1 Å). One should note that within the structures of *E. coli* DsbC and DsbG [48] there are no corresponding amino acid pairs that form hydrogen bonds across the β-strand and α-helix containing the active-site cysteines. Both these structures have been observed with a mixture of reduced and oxidized forms and, similar to *Mtb* DsbF, these proteins are more stable in their reduced forms (Figure 2c). In summary, the weak hydrogen bond between the amino acid pair Trp75 and Glu87 may, in part, contribute to the mixed redox state within the *Mtb* DsbF structure.

Biochemical analysis reveals that the physicochemical properties of *Mtb* DsbF is similar to *Mtb* DsbE [18]. Additionally, the *in vitro* activity assay indicates that *Mtb* DsbF, as with *Mtb* DsbE and *E. coli* DsbA, is capable of refolding reduced, unfolded hirudin, suggesting that it functions as a thiol oxidase. The reduced form of *Mtb* DsbF is more energetically stable compared to that of *Mtb* DsbE and the redox potential of *Mtb* DsbF active-site cysteines is −89 mV compared to −123 mV observed for *Mtb* DsbE [18], which is consistent with *Mtb* DsbF being a stronger oxidant than *Mtb* DsbE. The extensive hydrogen bonding network surrounding the solvent-protected Cys84 observed in the *Mtb* DsbF structure compared to the *Mtb* DsbE structure (Figures 6f and 6e respectively) could possibly stabilize the thiol form of Cys84 and thus favors *Mtb* DsbF's reduced state. Additionally, electrostatic surface potential analysis of the two *Mtb* Dsb proteins suggests that the surface potential surrounding the active site of *Mtb* DsbF is more positively charged facilitating the greater oxidizing redox potential and stabilizing the thiol form of the active site, whereas in the *Mtb* DsbE structure the surface potential suggests a mixed acidic and basic nature surrounding the active site which may lower the oxidizing redox potential compared to *Mtb* DsbF (Figures 6c and 6d).

Implications of transient *in vitro* interaction of *Mtb* DsbF and Rv1676

Co-expression studies, as well as their localization within the mycobacterial membrane or cell-wall, suggest that *Mtb* DsbF may aid in correct folding of Rv1676, a predicted peroxiredoxin. Peroxiredoxins are a ubiquitous family of antioxidant enzymes that have peroxidase activity and can be regulated by changes in phosphorylation, redox and possibly oligomerization states [49]. Peroxiredoxins have been shown to interact with thioredoxin-like folds [50] and more importantly, several lines of evidence have documented the ability of disulfide bond forming proteins to assist in folding peroxidases [51; 52]. Thus, an interaction between *Mtb* DsbF and Rv1676 is not unprecedented within the capacity of *Mtb* DsbF's potential role in ensuring

correct folding of Rv1676 in the membrane or cell-wall vicinity. The well-characterized *M. tuberculosis* Ahp system involved in antioxidant defense contains thioredoxin-like proteins and peroxiredoxins [53]. The gene expression patterns of AhpC (Rv2428) [54], a peroxiredoxin alkyl hydroperoxide reductase, its adaptor protein AhpD (Rv2429) [53], also annotated as an alkyl hydroperoxide reductase D, and a probable peroxiredoxin AhpE (Rv2238c) [55] were observed in addition to the *Mtb* Dsb systems (Figure 4b). Interestingly, the positively correlated genes within the Ahp system also have positive expression patterns with *Mtb* DsbF and Rv1676. These data suggest that, under oxidative stress, *Mtb* DsbF may potentially play a crucial role in detoxification whereby it may facilitate the correct folding of Rv1676. In contrast, they have anticorrelated expression patterns to the homolog of *Mtb* DsbF, *Mtb* DsbE and its potential redox partners.

M. tuberculosis extracytoplasmic sigma factors play a major role in altering patterns of gene expression to allow adaptation to stress responses during infection of its host, and upon entry into stationary phase [56; 57]. One of these sigma factors, SigL (Rv0735), upregulates polyketide synthases and secreted/membrane proteins, including the pair of proteins, *Mtb* DsbE (Rv2878c) and Rv2877c. Additionally, it has been demonstrated that a *sigL* mutant of *M. tuberculosis* is severely attenuated in a mouse model, suggesting that SigL (Rv0735) plays a role in virulence [40; 57]. Also, SigL has an anti-sigma factor, Rv0736 [57]. By association through correlated expression patterns with SigL and anti-SigL, *Mtb* DsbE may be involved in virulence and invasion whereas *Mtb* DsbF may be up-regulated under oxidative stress (Figure 4b). Our observation that two homologous proteins which have similar functions under distinct cellular conditions is not unprecedented. In plants, it has been shown that different thioredoxin isoforms function in different biological pathways, have different differential gene expression patterns, and different protein accumulation patterns in pea tissues, even though their sequence similarity is 60% identical at the amino acid level [58]. Thus, although *Mtb* DsbE and *Mtb* DsbF have both been shown to possess oxidase activity *in vitro*, the gene expression data infer that they may possibly function in separate biological pathways.

We have presented a study of *Mtb* DsbF which, despite its strong sequence homology and biochemical and structural similarity to *Mtb* DsbE, appears to function in distinct cellular contexts from *Mtb* DsbE, as shown by analysis of interacting partners and correlated gene expression. *Mtb* DsbE and *Mtb* DsbF likely assist in correct folding of disparate sets of disulfide bond containing secreted or cell-wall associated proteins in response to varying cellular conditions. This highlights the increasing need for understanding components of biological systems in terms of their context as well as simple homology relationships.

Methods and Materials

Cloning of *Rv1676* and *Rv1677*

M. tuberculosis Rv1676 and *Rv1677* genes were amplified from *M. tuberculosis* H37Rv genomic DNA using KOD HotStart Polymerase Kit (Novagen). For *Rv1676*, the 5′ primer (5′-GCCATATGGCTTGCCCTGAATGGGAAATTAGTCGATCG-3′) starts with the *Nde*I restriction site, which includes nucleotides 2-33 of *Rv1676*. The 3′ primer (5′-GCCTCGAGTCACTGAGTGCCCTTACCTC-3′) ends with the *Xho*I restriction site and contains the remaining 24 nucleotides of *Rv1676* including the stop-codon. For *Rv1677*, the 5′ primer (5′-GCGGATCCGCCACCCAGGTGCCGGCGGGCCAAACC-3′) starts with the *BamH*I restriction site which includes nucleotides 115-141 of *Rv1677*. The 3′ primer (5′-GCAAGCTTTCAACGGCTGGTTAACGCCGAGACGCGCCGCGTCAG-3′) ends with the *Hind*III restriction site and contains the remaining 36 nucleotides of *Rv1677* including the stop-codon. The resulting products were excised from a 2% agarose gel and purified using a gel extraction kit. The PCR products were ligated into a linearized blunt vector, pCR-BluntII-TOPO (Invitrogen), and then transformed into OneShot TOP10 *E. coli* cells (Invitrogen).

Presence of the correct genes were confirmed by DNA sequencing (Davis sequencing, Davis, CA).

Construction of the Expression Vector For *Rv1676*

Rv1676 was double-digested from the blunt vector with *Nde*I and *Xho*I, and the plasmid pET28a (+) (Novagen) was digested with the same restriction enzymes. The cut *Rv1676* gene was then ligated into cut pET28a(+) vector and transformed into *E. coli* BL21(DE3) cells (Novagen). Presence of the correct gene was confirmed by sequencing (Davis sequencing, Davis, CA).

Construction of the Expression Vector For *Rv1677*

Rv1677 was double-digested from the blunt vector with *BamH*I and *Hind*III, and the plasmid pETDuet-1 (Novagen) was digested with the same restriction enzymes. The cut *Rv1677* gene was then ligated into cut pETDuet vector and transformed into *E. coli* BL21(DE3) cells. Presence of the correct gene was confirmed by sequencing (Davis sequencing, Davis, CA) using primers specific to the pETDuet vector.

Construction of the Co-Expression Vector For *Rv1676* and *Rv1677*

Both full-length *Rv1676* from the blunt vector and pETDuet-Rv1677 were double-digested with *Nde*I and *Xho*I. Cut Rv1676 was ligated into cut pETDuet-Rv1677 vector and transformed into *E. coli* BL21(DE3) cells. Presence of the correct gene was confirmed by sequencing (Davis sequencing, Davis, CA) using primers specific to the pETDuet vector.

Overexpression, Purification and Crystallization of *Mtb* DsbF (Rv1677)

Mtb DsbF was purified from expression of pETDuet plasmid containing *Rv1677* gene using BL21(DE3) cells. Cells were grown aerobically at 37°C in LB medium containing 100 μg/mL ampicillin. Protein expression was induced by addition of 1 mM isopropyl-beta-D-thiogalactoside at an A_{OD600} of ~1.0 and cells harvested 4 h after induction. Cell harvesting, disruption and protein purification utilized the same protocols as described for Rv3607c [59]. The purified protein at 15 mg/ml was dialyzed into 50mM Tris/HCl pH 7.4 and 350mM NaCl for crystallization trials. The protein crystallized in 0.1 M Na-Malonate pH 7.0, 2.04 M Na-Citrate and 5% LDAO. Crystals were swiped through 1:1 crystallization condition and 50% glycerol, and diffraction data was collected at 70 K. Complete data sets were collected from single crystals.

Data collection, structure determination and refinement

Mtb DsbF native crystal diffracted to 1.6 Å with a unit cell dimensions of 100.1 × 100.1 × 30.1 Å with one monomer per asymmetric unit in space group $P4_22_12$. After autoindexing, images were indexed/integrated/reduced using DENZO and SCALEPACK [60]. Data collection statistics are presented in Table 1. The initial phases for the *Mtb* DsbF structure were determined by stochastic evolutionary programmed molecular replacement method (EPMR) [61] using a search model of *Mtb* DsbE (PDB code 1LU4) [18]. The EPMR solution was used for refinement carried out in CNS and model building which was carried out in O. The final rounds of refinement and addition of water molecules were carried out in SHELXL (http://shelx.uni-ac.gwdg.de/SHELX/). The CxxC active-site motif was in both its oxidized and reduced form, and was modeled as such. The final structure was complete from Val47 to Thr177 (which was modeled as Ala), where residues 39-46 and 178-182 are disordered and thus are missing from the model. The final data and refinement statistics are shown in Table 1, R_{work} and R_{free} were 14.4 and 20.0, respectively. The stereochemistry and geometry of each *Mtb* DsbF monomer was validated with PROCHECK [62] and ERRAT [63], and was found to be acceptable (*i.e.* no residues in the disallowed region of φ,ψ, space for *Mtb* DsbF model).

Oxidation and Reduction of *Mtb* DsbF

To oxidize *Mtb* DsbF, 50 mM of oxidized glutathioine (GSSG) was added to *Mtb* DsbF in 0.5 M NaCl and 0.1 M Tris.HCl, pH 7.4, and incubated for 1 hour at room temperature. The oxidized protein was then isolated by gel filtration chromatography in its original buffer. To reduce *Mtb* DsbF, 100 mM DTT was added to *Mtb* DsbF in 0.5 M NaCl and 0.1 M Tris.HCl, pH 7.4, and incubated overnight at 4°C. The reduced protein was then isolated by gel filtration chromatography in its original buffer.

Redox Properties of *Mtb* DsbF - Comparison to Glutathione

The *in vitro* redox state of *Mtb* DsbF was assayed as described previously [64; 65; 66]. In this assay, the change in fluorescence intensity (excitation wavelength 280 nm) was measured at the wavelength of maximum emission (356 nm for *Mtb* DsbF). Experiments were carried out in 100 mM sodium phosphate, pH 7.0, and 1.0 mM EDTA. Oxidized and reduced 5 μM *Mtb* DsbF were incubated at 25°C in the presence of 0.1 mM GSSG and varying concentration of GSH (0 - 10 mM) for 12 hr before recording the fluorescence emission on a Spex Fluorolog (Jubin Yvon-Spex). The equilibrium concentrations of GSH and GSSG were calculated as described [18]. The equilibrium constant K_{eq} was estimated from nonlinear regression analysis of the data according to the Nernst equation, and from the equilibrium constant and by using the glutathione standard potential ($E'_{0GSH/GSSG}$ = -240 mV) [32] the standard redox potential (E'_0) was calculated as described [18].

Determination of pK_a of Cys81

The pH-dependent ionization of the Cys81 thiol (solvent-exposed) was followed by the specific absorbance of the thiolate anion at 240 nm as described earlier [25]. As a control, the pH-dependent absorbance for the oxidized form of *Mtb* DsbF was recorded. To avoid precipitation artifacts and to minimize buffer absorbance, a buffer system consisting of 10 mM K_2PO_4, 10 mM boric acid, 10 mM sodium succinate, 1 mM EDTA and 200 mM KCl (containing 100 μM DTT for the reduced protein) was used. The pH (initial value, 8.5) was lowered to 2.2 by stepwise addition of aliquots of 0.1 M HCl, and the absorbance at 240 and 280 nm was recorded and corrected for the volume increase. Samples had an average initial protein concentration of approximately 30 μM. The pH dependence of the thiolate-specific absorbance signal was fitted according to the Henderson-Hasselbalch equation as described previously [18].

Determination of unfolding/folding equilibrium

The reversible guanidine hydrochloride (GdnHCl)-induced unfolding/folding of *Mtb* DsbF was performed by measuring the CD ellipticities at 222 nm [67]. The spectra of the reduced form were recorded in the presence of 0.5 mM DTT. For unfolding equilibrium, *Mtb* DsbF (final concentration of 7 μM) was dissolved in different concentrations of GdnHCl and incubated for 3 h at 25°C. Data were analyzed according to the two-state assumption [27; 68]. The standard changes of folding free energy and the difference in stability between the oxidized and reduced forms of DsbF protein were calculated as described previously [18].

Oxidase activity of *Mtb* DsbF - refolding of hirudin

Commercial *Hirudo medicinalis* hirudin (Sigma) was purified to remove contaminants by reverse-phase HPLC on a polymeric column (PLRP/S; 300A, 5 μm bead; 2 mm × 15 cm) at a flow rate of 100 μL/min. Solvents A and B used for reverse-phase HPLC were 0.1% trifluoroacetic acid in water and acetonitrile, respectively. HPLC purified hirudin was reduced and unfolded as described [69], and then reduced, unfolded hirudin (5 pmol) was refolded with stoichiometric amounts of oxidized *Mtb* DsbF (5 pmol) in 100 mM ammonium bicarbonate, pH 8.0 at 25 °C. Each 10 μL reaction was quenched at different time points by incubating initially with 50 μL 6M GdnHCl for 10 minutes at 50 °C followed by 0.5 μL 100 mM

iodoacetamide for 15 mins at 25 °C. The samples were then desalted with ZipTipC4 (Millipore) before analysis with MALDI-TOF (Voyager). Experiments were repeated no protein added and with similar quantities (5 pmol) of *Mtb* DsbE, *E. coli* DsbA and *E. coli* thioredoxin as positive and negative controls, respectively.

Expression and purification of Rv1676

Rv1676 was purified from expression of pET28a(+) plasmid containing *Rv1676* gene using BL21(DE3) cells. Cells were grown aerobically at both 18°C and 37°C in LB medium containing 100 μg/mL kanamycin. Protein expression was induced by addition of 1 mM isopropyl-beta-D-thiogalactoside at an $A_{OD6}00$ of ~1.0 and cells harvested between 2h, 4h and overnight after induction. Cell harvesting, disruption, solubility tests and protein purification in 6M GdnHCl were carried out as described previously [70]. Attempts were made to refold the Rv1676 by step-wise dialysis from 6M GdnHCl to native buffer (50 mM Tris pH 7.4, 150 mM NaCl).

Co-expression of Rv1676 and Rv1677 (DsbF)

The pETDuet co-expression plasmid containing *Rv1676* and *Rv1677* was transformed into BL21(DE3) cells. Cells were grown aerobically at 37°C in LB medium to an A_{OD600} of ~0.8 then protein expression was induced by addition of 1 mM IPTG and the cells were harvested 4 h after induction. Cells were harvested, lyzed and the supernatant extracted as for Rv1677. The supernatant was loaded onto a Ni^{2+} charged HiTrap chelating column. The column was washed with 20 mM Hepes, pH 7.8 and 150 mM NaCl, and eluted with a linear gradient of imidazole from 0 to 500 mM in 20 mM Hepes pH 7.8 and 150 mM NaCl. The fractions were analyzed by SDS-PAGE gel. The fraction that corresponds to both Rv1676 and Rv1677 proteins were analyzed by mass spectrometry.

Analysis of tryptic peptide sequence tags by micro-liquid chromatography tandem mass spectrometry (μLC-MSMS)

Samples were analyzed by μLC-MSMS with data-dependent acquisition (LCQ-DECA, ThermoFinnigan, San Jose, California) after dissolution in 5 μL 70 % acetic acid (v/v). A reverse-phase column (200 μm × 10 cm; PLRP/S 5 μm, 300 Å; Michrom Biosciences, San Jose) was equilibrated for 10 minutes at 1.5 μL/min with 95% A, 5% B (A, 0.1% formic acid in water; B, 0.1% formic acid in acetonitrile) prior to sample injection. A linear gradient was initiated 10 min after sample injection ramping to 60% A, 40% B after 50 minutes and 20% A, 80% B after 65 minutes. Column eluent was directed to a coated glass electrospray emitter (TaperTip, TT150-50-50-CE-5, New Objective) at 3.3 kV for ionization without nebulizer gas. The mass spectrometer was operated in 'triple-play' mode with a survey scan (400-1500 m/z), data-dependent zoom scan, and MSMS with exclusion of singly-charged ions. Individual sequencing experiments were matched to a custom *M. tuberculosis* sequence database downloaded from The Sanger Center using Sequest software (ThermoFinnigan, San Jose). The search was run under the 'no enzyme' mode to identify non-tryptic peptides. The results of Sequest searches were carefully scrutinized. MSMS spectra of doubly charged ions with cross correlation scores (Xcorr) greater than 2.8 and triply charged ions with scores over 3.2 were examined manually. Some noisy spectra were discarded despite high Xcorr scores. Non-tryptic peptide returns were retained only if the data had particularly high signal to noise.

Genome-wide analysis of *Mtb* gene coexpression

This methodology has been previously described[45], so in brief, four published gene expression datasets from *M. tuberculosis* strain H37Rv were collected [41; 42; 43; 44] from the Gene Expression Omnibus (GEO) (PMID: 17099226). Gene expression data from the four studies were represented as a matrix where the rows were genes and the columns were experiments.

To construct an expression vector for a gene, the data from each of the four studies were concatenated. Correlation coefficients of gene expression vectors were calculated for all possible pairs of genes. To obtain a correlation coefficient for genes x and y over N experiments, the Pearson correlation coefficient, r_{xy}, was calculated as:

$$r_{xy} = \frac{\sum_{\text{experiment}}^{N} (x_i - \mu_x)(y_i - \mu_y)}{(N-1)s_x s_y}$$

where x_i and y_i are the log expression values reported in the GEO data file, μ_x and μ_y are the means of the values in the combined vector, s_x and s_y are the standard deviations. For each pair of genes analyzed, combined expression vectors were truncated to include only those experiments for which measurements were obtained for both genes. Thus N was adjusted for each pair of genes assessed. In all, 553 experiments were included for the analysis of 3,925 *Mtb* genes to infer some 7,700,000 pairwise coexpression relationships between pairs of genes.

Acknowledgments

This work has been supported by a grant from the National Institutes of Health, DOE-BER and HHMI (for D.E.) and National Institutes of Health (P01AIO68135, subcontract for C.W.G.) The authors thank Dr John T. Belisle, Colorado State University, NIH, NIAID Contract NO1 A1-75320 for generous supply of *M. tuberculosis* H37Rv genomic DNA. We also thank Drs. Michael Sawaya and Duilio Cascio for invaluable help with data collection and general crystallography. Finally, special thanks to Morgan Beeby for helpful comments.

References

1. Martin JL. Thioredoxin--a fold for all reasons. Structure 1995;3:245–50. [PubMed: 7788290]
2. Schroder E, Ponting CP. Evidence that peroxiredoxins are novel members of the thioredoxin fold superfamily. Protein Sci 1998;7:2465–8. [PubMed: 9828014]
3. Missiakas D, Raina S. Protein folding in the bacterial periplasm. J Bacteriol 1997;179:2465–71. [PubMed: 9098040]
4. Zhang HZ, Donnenberg MS. DsbA is required for stability of the type IV pilin of enteropathogenic *Escherichia coli*. Mol Microbiol 1996;21:787–97. [PubMed: 8878041]
5. Zav'yalov VP, Chernovskaya TV, Chapman DA, Karlyshev AV, MacIntyre S, Zavialov AV, Vasiliev AM, Denesyuk AI, Zav'yalova GA, Dudich IV, Korpela T, Abramov VM. Influence of the conserved disulphide bond, exposed to the putative binding pocket, on the structure and function of the immunoglobulin-like molecular chaperone Caf1M of *Yersinia pestis*. Biochem J 1997;324(Pt 2):571–8. [PubMed: 9182720]
6. Yu J, Kroll JS. DsbA: a protein-folding catalyst contributing to bacterial virulence. Microbes Infect 1999;1:1221–8. [PubMed: 10580278]
7. Hu SH, Peek JA, Rattigan E, Taylor RK, Martin JL. Structure of TcpG, the DsbA protein folding catalyst from *Vibrio cholerae*. J Mol Biol 1997;268:137–46. [PubMed: 9149147]
8. Manning PA. The tcp gene cluster of *Vibrio cholerae*. Gene 1997;192:63–70. [PubMed: 9224875]
9. Bardwell JC, McGovern K, Beckwith J. Identification of a protein required for disulfide bond formation *in vivo*. Cell 1991;67:581–9. [PubMed: 1934062]
10. Joly JC, Swartz JR. *In vitro* and *in vivo* redox states of the *Escherichia coli* periplasmic oxidoreductases DsbA and DsbC. Biochemistry 1997;36:10067–72. [PubMed: 9254601]
11. Bader M, Muse W, Ballou DP, Gassner C, Bardwell JC. Oxidative protein folding is driven by the electron transport system. Cell 1999;98:217–27. [PubMed: 10428033]
12. Missiakas D, Georgopoulos C, Raina S. Identification and characterization of the *Escherichia coli* gene dsbB, whose product is involved in the formation of disulfide bonds *in vivo*. Proc Natl Acad Sci U S A 1993;90:7084–8. [PubMed: 7688471]

13. Grovc J, Busby S, Cole J. The role of the genes nrf EFG and ccmFH in cytochrome c biosynthesis in *Escherichia coli*. Mol Gen Genet 1996;252:332–41. [PubMed: 8842153]

14. Reid E, Cole J, Eaves DJ. The *Escherichia coli* CcmG protein fulfils a specific role in cytochrome c assembly. Biochem J 2001;355:51–8. [PubMed: 11256948]

15. Fabianek RA, Hofer T, Thony-Meyer L. Characterization of the *Escherichia coli* CcmH protein reveals new insights into the redox pathway required for cytochrome c maturation. Arch Microbiol 1999;171:92–100. [PubMed: 9914305]

16. Stewart EJ, Katzen F, Beckwith J. Six conserved cysteines of the membrane protein DsbD are required for the transfer of electrons from the cytoplasm to the periplasm of *Escherichia coli*. Embo J 1999;18:5963–71. [PubMed: 10545108]

17. Gruber CW, Cemazar M, Heras B, Martin JL, Craik DJ. Protein disulfide isomerase: the structure of oxidative folding. Trends Biochem Sci 2006;31:455–64. [PubMed: 16815710]

18. Goulding CW, Apostol MI, Gleiter S, Parseghian A, Bardwell J, Gennaro M, Eisenberg D. Gram-positive DsbE proteins function differently from Gram-negative DsbE homologs. A structure to function analysis of DsbE from *Mycobacterium tuberculosis*. J Biol Chem 2004;279:3516–24. [PubMed: 14597624]

19. Goldstone D, Baker EN, Metcalf P. Crystallization and preliminary diffraction studies of the C-terminal domain of the DipZ homologue from *Mycobacterium tuberculosis*. Acta Crystallograph Sect F Struct Biol Cryst Commun 2005;61:243–5.

20. Hoffmann C, Leis A, Niederweis M, Plitzko JM, Engelhardt H. Disclosure of the mycobacterial outer membrane: cryo-electron tomography and vitreous sections reveal the lipid bilayer structure. Proc Natl Acad Sci U S A 2008;105:3963–7. [PubMed: 18316738]

21. Raviglione MC, Snider DE Jr, Kochi A. Global epidemiology of tuberculosis. Morbidity and mortality of a worldwide epidemic. Jama 1995;273:220–6. [PubMed: 7807661]

22. Pablos-Mendez A, Raviglione MC, Laszlo A, Binkin N, Rieder HL, Bustreo F, Cohn DL, Lambregts-van Weezenbeek CS, Kim SJ, Chaulet P, Nunn P. Global surveillance for antituberculosis-drug resistance, 1994-1997. World Health Organization-International Union against Tuberculosis and Lung Disease Working Group on Anti-Tuberculosis Drug Resistance Surveillance. N Engl J Med 1998;338:1641–9. [PubMed: 9614254]

23. Goulding CW, Perry LJ, Anderson D, Sawaya MR, Cascio D, Apostol MI, Chan S, Parseghian A, Wang SS, Wu Y, Cassano V, Gill HS, Eisenberg D. Structural genomics of *Mycobacterium tuberculosis*: a preliminary report of progress at UCLA. Biophys Chem 2003;105:361–70. [PubMed: 14499904]

24. Goulding CW, Apostol M, Anderson DH, Gill HS, Smith CV, Kuo MR, Yang JK, Waldo GS, Suh SW, Chauhan R, Kale A, Bachhawat N, Mande SC, Johnston JM, Lott JS, Baker EN, Arcus VL, Leys D, McLean KJ, Munro AW, Berendzen J, Sharma V, Park MS, Eisenberg D, Sacchettini J, Alber T, Rupp B, Jacobs W Jr, Terwilliger TC. The TB structural genomics consortium: providing a structural foundation for drug discovery. Curr Drug Targets Infect Disord 2002;2:121–41. [PubMed: 12462144]

25. Li Q, Hu H, Xu G. Biochemical characterization of the thioredoxin domain of *Escherichia coli* DsbE protein reveals a weak reductant. Biochem Biophys Res Commun 2001;283:849–53. [PubMed: 11350062]

26. Martin JL, Bardwell JC, Kuriyan J. Crystal structure of the DsbA protein required for disulphide bond formation *in vivo*. Nature 1993;365:464–8. [PubMed: 8413591]

27. Wunderlich M, Glockshuber R. Redox properties of protein disulfide isomerase (DsbA) from *Escherichia coli*. Protein Sci 1993;2:717–26. [PubMed: 8495194]

28. Zapun A, Bardwell JC, Creighton TE. The reactive and destabilizing disulfide bond of DsbA, a protein required for protein disulfide bond formation *in vivo*. Biochemistry 1993;32:5083–92. [PubMed: 8494885]

29. Cole ST, Brosch R, Parkhill J, Garnier T, Churcher C, Harris D, Gordon SV, Eiglmeier K, Gas S, Barry CE 3rd, Tekaia F, Badcock K, Basham D, Brown D, Chillingworth T, Connor R, Davies R, Devlin K, Feltwell T, Gentles S, Hamlin N, Holroyd S, Hornsby T, Jagels K, Krogh A, McLean J, Moule S, Murphy L, Oliver K, Osborne J, Quail MA, Rajandream MA, Rogers J, Rutter S, Seeger K, Skelton J, Squares R, Squares S, Sulston JE, Taylor K, Whitehead S, Barrell BG. Deciphering the

biology of *Mycobacterium tuberculosis* from the complete genome sequence. Nature 1998;393:537–44. [PubMed: 9634230]

30. Emanuelsson O, Brunak S, von Heijne G, Nielsen H. Locating proteins in the cell using TargetP, SignalP and related tools. Nat Protoc 2007;2:953–71. [PubMed: 17446895]
31. Musil D, Zucic D, Turk D, Engh RA, Mayr I, Huber R, Popovic T, Turk V, Towatari T, Katunuma N, et al. The refined 2.15 A X-ray crystal structure of human liver cathepsin B: the structural basis for its specificity. Embo J 1991;10:2321–30. [PubMed: 1868826]
32. Aslund F, Berndt KD, Holmgren A. Redox potentials of glutaredoxins and other thiol-disulfide oxidoreductases of the thioredoxin superfamily determined by direct protein-protein redox equilibria. J Biol Chem 1997;272:30780–6. [PubMed: 9388218]
33. Van Dorsselaer A, Lepage P, Bitsch F, Whitechurch O, Riehl-Bellon N, Fraisse D, Green B, Roitsch C. Mass spectrometry analyses of recombinant hirudins (7 kDa). Biochemistry 1989;28:2949–56. [PubMed: 2742822]
34. Chivers PT, Prehoda KE, Volkman BF, Kim BM, Markley JL, Raines RT. Microscopic pKa values of *Escherichia coli* thioredoxin. Biochemistry 1997;36:14985–91. [PubMed: 9398223]
35. Grauschopf U, Winther JR, Korber P, Zander T, Dallinger P, Bardwell JC. Why is DsbA such an oxidizing disulfide catalyst? Cell 1995;83:947–55. [PubMed: 8521518]
36. Strong M, Mallick P, Pellegrini M, Thompson MJ, Eisenberg D. Inference of protein function and protein linkages in *Mycobacterium tuberculosis* based on prokaryotic genome organization: a combined computational approach. Genome Biol 2003;4:R59. [PubMed: 12952538]
37. Marcotte EM, Pellegrini M, Thompson MJ, Yeates TO, Eisenberg D. A combined algorithm for genome-wide prediction of protein function. Nature 1999;402:83–6. [PubMed: 10573421]
38. Bowers PM, Pellegrini M, Thompson MJ, Fierro J, Yeates TO, Eisenberg D. Prolinks: a database of protein functional linkages derived from coevolution. Genome Biol 2004;5:R35. [PubMed: 15128449]
39. Gu S, Chen J, Dobos KM, Bradbury EM, Belisle JT, Chen X. Comprehensive proteomic profiling of the membrane constituents of a *Mycobacterium tuberculosis* strain. Mol Cell Proteomics 2003;2:1284–96. [PubMed: 14532352]
40. Hahn MY, Raman S, Anaya M, Husson RN. The *Mycobacterium tuberculosis* extracytoplasmic-function sigma factor SigL regulates polyketide synthases and secreted or membrane proteins and is required for virulence. J Bacteriol 2005;187:7062–71. [PubMed: 16199577]
41. Boshoff HI, Myers TG, Copp BR, McNeil MR, Wilson MA, Barry CE 3rd. The transcriptional responses of *Mycobacterium tuberculosis* to inhibitors of metabolism: novel insights into drug mechanisms of action. J Biol Chem 2004;279:40174–84. [PubMed: 15247240]
42. Boshoff HI, Reed MB, Barry CE 3rd, Mizrahi V. DnaE2 polymerase contributes to *in vivo* survival and the emergence of drug resistance in *Mycobacterium tuberculosis*. Cell 2003;113:183–93. [PubMed: 12705867]
43. Gao Q, Kripke K, Arinc Z, Voskuil M, Small P. Comparative expression studies of a complex phenotype: cord formation in *Mycobacterium tuberculosis*. Tuberculosis (Edinb) 2004;84:188–96. [PubMed: 15207488]
44. Gao Q, Kripke KE, Saldanha AJ, Yan W, Holmes S, Small PM. Gene expression diversity among *Mycobacterium tuberculosis* clinical isolates. Microbiology 2005;151:5–14. [PubMed: 15632420]
45. Riley R, Pellegrini M, Eisenberg D. Identifying cognate binding pairs among a large set of paralogs: the case of PE/PPE proteins of *Mycobacterium tuberculosis*. PLoS Comput Biol 2008;4:e1000174. [PubMed: 18787688]
46. Guddat LW, Bardwell JC, Martin JL. Crystal structures of reduced and oxidized DsbA: investigation of domain motion and thiolate stabilization. Structure 1998;6:757–67. [PubMed: 9655827]
47. Edeling MA, Guddat LW, Fabianek RA, Thony-Meyer L, Martin JL. Structure of CcmG/DsbE at 1.14 A resolution: high-fidelity reducing activity in an indiscriminately oxidizing environment. Structure 2002;10:973–9. [PubMed: 12121652]
48. Heras B, Edeling MA, Schirra HJ, Raina S, Martin JL. Crystal structures of the DsbG disulfide isomerase reveal an unstable disulfide. Proc Natl Acad Sci U S A 2004;101:8876–81. [PubMed: 15184683]

49. Wood ZA, Schroder E, Robin Harris J, Poole LB. Structure, mechanism and regulation of peroxiredoxins. Trends Biochem Sci 2003;28:32–40. [PubMed: 12517450]
50. Barranco-Medina S, Krell T, Bernier-Villamor L, Sevilla F, Lazaro JJ, Dietz KJ. Hexameric oligomerization of mitochondrial peroxiredoxin PrxIIF and formation of an ultrahigh affinity complex with its electron donor thioredoxin Trx-o. J Exp Bot 2008;59:3259–69. [PubMed: 18632730]
51. Kurokawa Y, Yanagi H, Yura T. Overexpression of protein disulfide isomerase DsbC stabilizes multiple-disulfide-bonded recombinant protein produced and transported to the periplasm in *Escherichia coli*. Appl Environ Microbiol 2000;66:3960–5. [PubMed: 10966415]
52. Miyazaki-Imamura C, Oohira K, Kitagawa R, Nakano H, Yamane T, Takahashi H. Improvement of H_2O_2 stability of manganese peroxidase by combinatorial mutagenesis and high-throughput screening using *in vitro* expression with protein disulfide isomerase. Protein Eng 2003;16:423–8. [PubMed: 12874375]
53. Bryk R, Lima CD, Erdjument-Bromage H, Tempst P, Nathan C. Metabolic enzymes of mycobacteria linked to antioxidant defense by a thioredoxin-like protein. Science 2002;295:1073–7. [PubMed: 11799204]
54. Guimaraes BG, Souchon H, Honore N, Saint-Joanis B, Brosch R, Shepard W, Cole ST, Alzari PM. Structure and mechanism of the alkyl hydroperoxidase AhpC, a key element of the *Mycobacterium tuberculosis* defense system against oxidative stress. J Biol Chem 2005;280:25735–42. [PubMed: 15886207]
55. Li S, Peterson NA, Kim MY, Kim CY, Hung LW, Yu M, Lekin T, Segelke BW, Lott JS, Baker EN. Crystal Structure of AhpE from *Mycobacterium tuberculosis*, a 1-Cys peroxiredoxin. J Mol Biol 2005;346:1035–46. [PubMed: 15701515]
56. Rodrigue S, Provvedi R, Jacques PE, Gaudreau L, Manganelli R. The sigma factors of *Mycobacterium tuberculosis*. FEMS Microbiol Rev 2006;30:926–41. [PubMed: 17064287]
57. Dainese E, Rodrigue S, Delogu G, Provvedi R, Laflamme L, Brzezinski R, Fadda G, Smith I, Gaudreau L, Palu G, Manganelli R. Posttranslational regulation of *Mycobacterium tuberculosis* extracytoplasmic-function sigma factor sigma L and roles in virulence and in global regulation of gene expression. Infect Immun 2006;74:2457–61. [PubMed: 16552079]
58. Traverso JA, Vignols F, Cazalis R, Pulido A, Sahrawy M, Cejudo FJ, Meyer Y, Chueca A. PsTRXh1 and PsTRXh2 are both pea h-type thioredoxins with antagonistic behavior in redox imbalances. Plant Physiol 2007;143:300–11. [PubMed: 17098852]
59. Goulding CW, Apostol MI, Sawaya MR, Phillips M, Parseghian A, Eisenberg D. Regulation by oligomerization in a mycobacterial folate biosynthetic enzyme. J Mol Biol 2005;349:61–72. [PubMed: 15876368]
60. Otwinowski Z, Minor W. Processing of X-ray diffraction data collected in oscillation mode. Methods Enzymol 1997;276:307–326.
61. Kissinger CR, Gehlhaar DK, Smith BA, Bouzida D. Molecular replacement by evolutionary search. Acta Crystallogr D Biol Crystallogr 2001;57:1474–9. [PubMed: 11567162]
62. Laskowski RA, Moss DS, Thornton JM. Main-chain bond lengths and bond angles in protein structures. J Mol Biol 1993;231:1049–67. [PubMed: 8515464]
63. Colovos C, Yeates TO. Verification of protein structures: patterns of nonbonded atomic interactions. Protein Sci 1993;2:1511–9. [PubMed: 8401235]
64. Loferer H, Wunderlich M, Hennecke H, Glockshuber R. A bacterial thioredoxin-like protein that is exposed to the periplasm has redox properties comparable with those of cytoplasmic thioredoxins. J Biol Chem 1995;270:26178–83. [PubMed: 7592822]
65. Rossmann R, Stern D, Loferer H, Jacobi A, Glockshuber R, Hennecke H. Replacement of Pro109 by His in TlpA, a thioredoxin-like protein from *Bradyrhizobium japonicum*, alters its redox properties but not its *in vivo* functions. FEBS Lett 1997;406:249–54. [PubMed: 9136895]
66. Bessette PH, Aslund F, Beckwith J, Georgiou G. Efficient folding of proteins with multiple disulfide bonds in the *Escherichia coli* cytoplasm. Proc Natl Acad Sci U S A 1999;96:13703–8. [PubMed: 10570136]

67. Hennecke J, Spleiss C, Glockshuber R. Influence of acidic residues and the kink in the active-site helix on the properties of the disulfide oxidoreductase DsbA. J Biol Chem 1997;272:189–95. [PubMed: 8995246]

68. Santoro MM, Bolen DW. Unfolding free energy changes determined by the linear extrapolation method. 1. Unfolding of phenylmethanesulfonyl alpha-chymotrypsin using different denaturants. Biochemistry 1988;27:8063–8. [PubMed: 3233195]

69. Hennecke J, Sebbel P, Glockshuber R. Random circular permutation of DsbA reveals segments that are essential for protein folding and stability. J Mol Biol 1999;286:1197–215. [PubMed: 10047491]

70. Goulding CW, Perry LJ. Protein production in *Escherichia coli* for structural studies by X-ray crystallography. J Struct Biol 2003;142:133–43. [PubMed: 12718925]

Abbreviations used

Mtb	*Mycobacterium tuberculosis*
E. coli	*Escherichia coli*
Rv number	Sanger center notation for each gene in *Mtb*
TB	tuberculosis
Dsb	disulfide bond forming proteins
rmsd	root mean square deviation function
TFA	trifluoroacetic acid
IPTG	isopropyl-beta-D-thiogalactoside

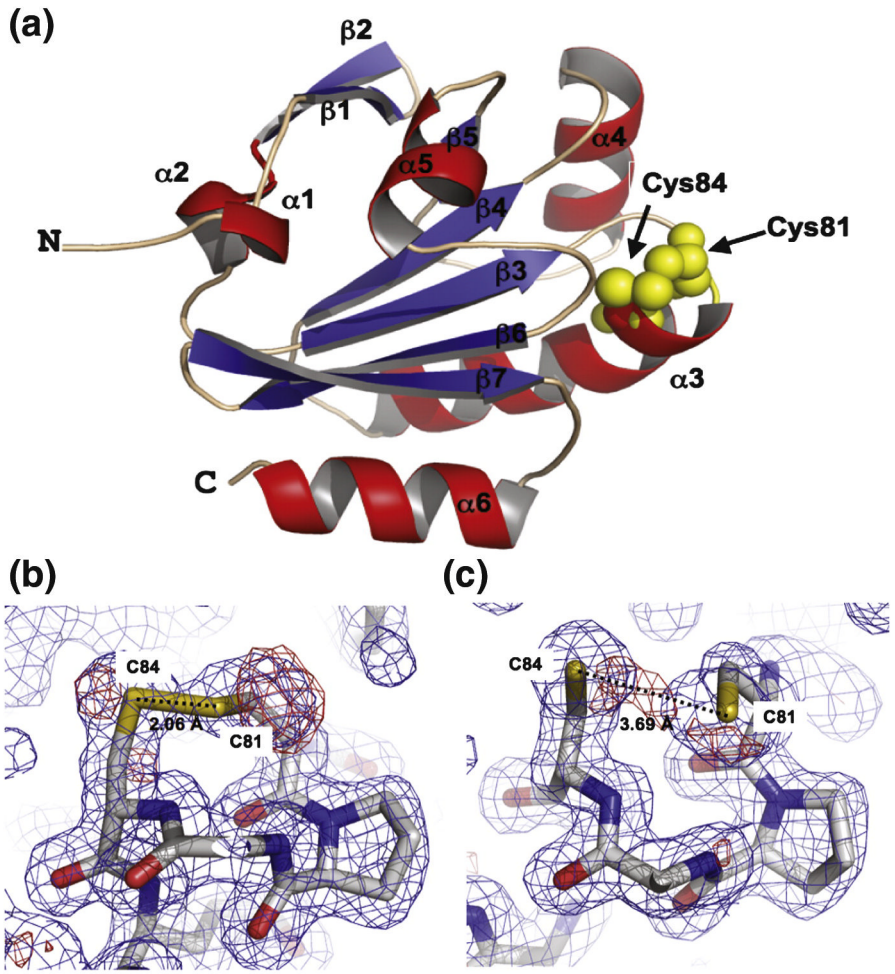

Figure 1.

(a) Structure of *Mtb* DsbF in its oxidized form is shown as a ribbon diagram. The β-sheets, α-helices and random coil are colored blue, red and cream, respectively. The atoms for the two active-site cysteines, Cys81 and Cys84 are colored in yellow. (b) and (c) Electron density surrounding the active-site CxxC motif of *Mtb* DsbF where the cysteines are modeled in both the (b) oxidized and (c) reduced forms. The 2*fo-fc* electron density mesh (blue) and the *fo-fc* negative density mesh (red) are contoured at sigma 3.0. Shown are stick cartoons of the active-site where the carbon, oxygen, nitrogen and sulfur atoms are colored in white, red, blue and yellow, respectively.

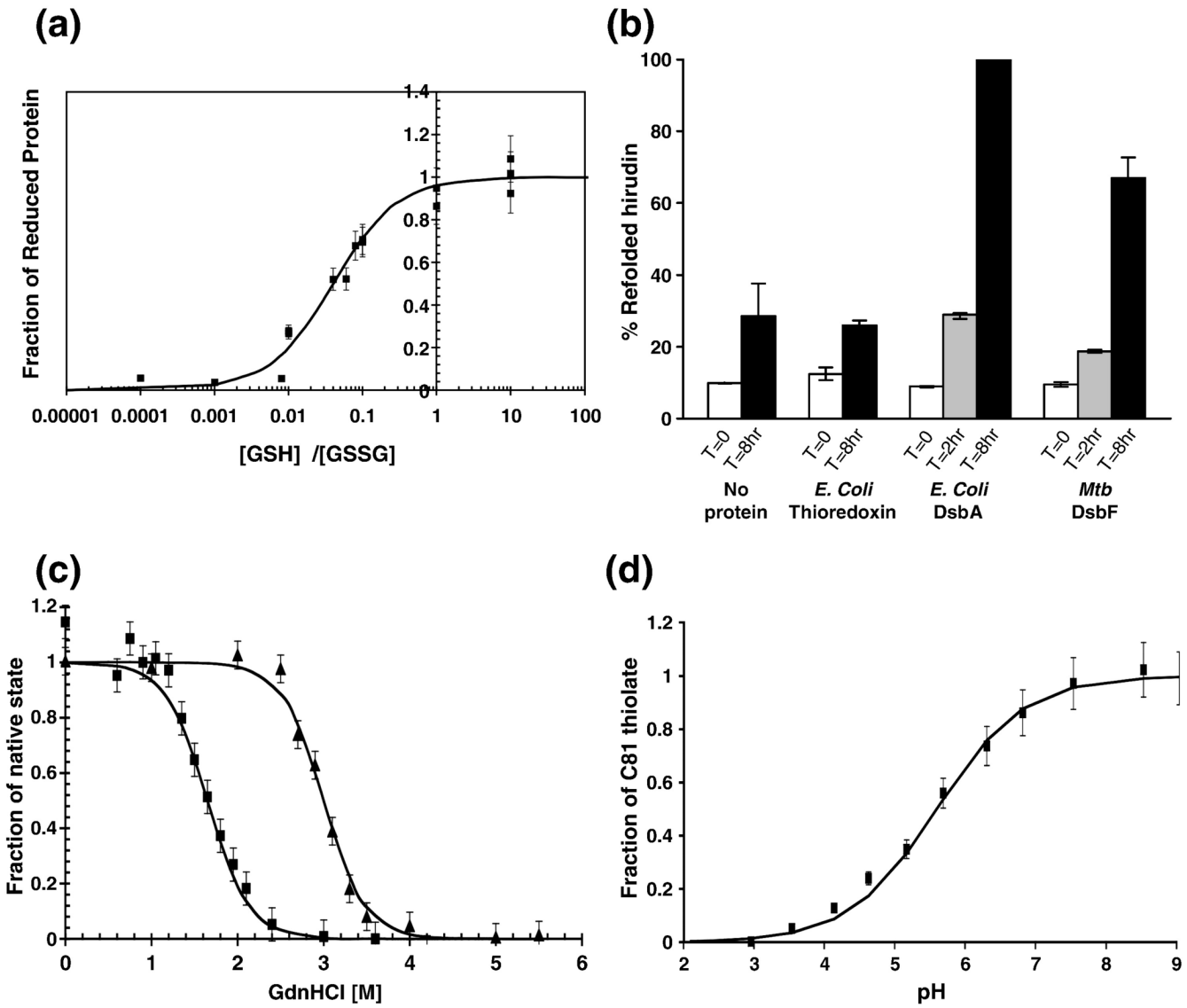

Figure 2.

Biochemical characterization of *Mtb* DsbF. (a) Redox equilibrium of *Mtb* DsbF with glutathione. The y-axis represents the proportion of *Mtb* DsbF present in the reduced form at equilibrium with various mixtures of reduced (GSH) and oxidized (GSSG) glutathione (x-axis), which was measured by exploiting the difference in fluorescence (347 nm) of reduced *Mtb* DsbF compared to oxidized *Mtb* DsbF. Equilibrium concentrations of oxidized and reduced *Mtb* DsbF and GSH and GSSG were calculated as described [66]. The equilibrium constant was calculated to be 40 ± 5 μM, which is consistent with *Mtb* DsbF acting as an oxidant. (b) Analysis of the refolding activity of reduced and unfolded hirudin. 5 pmol reduced, unfolded hirudin was incubated alone or with stoichiometric quantities (5 pmol) of *Mtb* DsbF, *E. coli* DsbA and *E. coli* thioredoxin. Samples were removed as indicated at each time point and the reactions, quenched by the addition of iodoacetamide, were analyzed by MALDI-TOF mass spectrometry. The appearance of native hirudin (*m/z* 6765) is represented as a percentage of the total intensities of native and carbamidomethylated hirudin. (c) GdnHCl-dependent unfolding/folding of *Mtb* DsbF. Guanidine hydrochloride (GdnHCl)-dependent unfolding was monitored by circular dichroism spectroscopy at 222 nm for oxidized *Mtb* DsbF (shown as

squares) and reduced *Mtb* DsbF (shown as triangles). Since the reduced form of *Mtb* DsbF unfolds at higher concentrations of GdnHCl than the oxidized form, the reduced form of *Mtb* DsbF is its more stable form. (d) Determination of the pK_a value of the active-site cysteine, Cys81, in *Mtb* DsbF. The absorption specific to reduced *Mtb* DsbF protein is shown as a function of pH (x-axis) compared to the fraction of Cys81 thiolate (y-axis). The pK_a of Cys81 was calculated by fitting the data points as described [67]. The pK_a of Cys81 in *Mtb* DsbF is 5.6 ± 0.3.

(a)

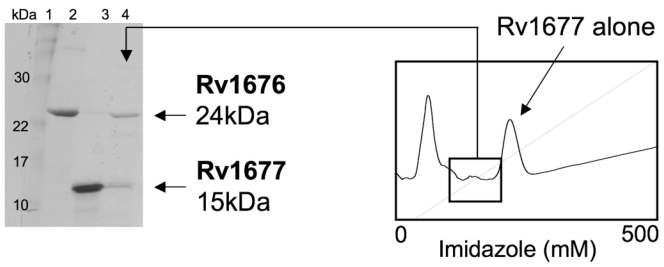

(b)

Rv1676	Peptide	Mass	Charge	Cross-Correlation	
1800	R.HQEVADSGITEVVFFHSAADALR.G	2500.71	3	6.99	6/11
1656 - 1665	R.HADDQWSVDQLIDINR.S	1926.04	2	6.23	5/6
1803	R.HQEVADSGITEVVFFHSAADALR.G	2500.71	2	4.98	13/22
1179	R.LQDINDQPVDVPAATGR.T	1809.96	2	4.72	3/4
1185 - 1188	R.LQDINDQPVDVPAATGR.T	1809.96	2	4.29	25/32
1944	R.GYQSLLPFAVIADPDRVQYR.E	2309.61	2	3.42	9/19
1938	R.GYQSLLPFAVIADPDRVQYR.E	2309.61	2	3.32	7/38
1014 - 1026	R.YGIGVPTR.L	863.00	1	1.64	5/7

(c)

Rv1676 - Trypsin

From To	Mol Wt	From To	Mol Wt	From To	Mol Wt
1 - 10	1203.4	51 - 57	700.8	143 - 148	707.8
11 - 12	233.3	58 - 58	174.2	149 - 157	951.1
13 - 13	174.2	59 - 75	1808.9	158 - 164	785.9
14 - 15	275.3	76 - 81	800.9	165 - 172	842.0
16 - 22	865.1	82 - 82	174.2	173 - 177	629.6
23 - 31	1014.1	83 - 94	1380.7	178 - 210	3271.6
32 - 39	1022.2	95 - 99	593.6	211 - 226	1925.0
40 - 47	862.0	100 - 122	2499.7	227 - 231	460.5
48 - 50	358.4	123 - 138	1762.0	232 - 234	304.3
		139 - 142	564.6		

Figure 3.

Co-expression studies for *Mtb* DsbF with Rv1676. (a) Purified Rv1676 and *Mtb* DsbF complex. On the right is the chromatograph of the Ni^{2+} affinity column elution (0 – 500 mM imidazole) of Rv1676 and *Mtb* DsbF co-expression experiment and the SDS-PAGE gel shows lanes 1) protein ladder; 2) Rv1676 purified in denaturing conditions (6M urea); 3) *Mtb* DsbF purified under native conditions and; 4) eluted Rv1676 and *Mtb* DsbF complex. The eluted Rv1676 and *Mtb* DsbF bands correspond to a small peak before the larger elution of pure *Mtb* DsbF alone. (b) Mass spectrometry results from a co-elution fraction of trypsin digested *Mtb* DsbF and Rv1676. The peptide fragments correspond to Rv1676 with high significance. (c) Predicted trypsin peptide map of Rv1676. Highlighted in grey are the peptides identified experimentally in 3b.

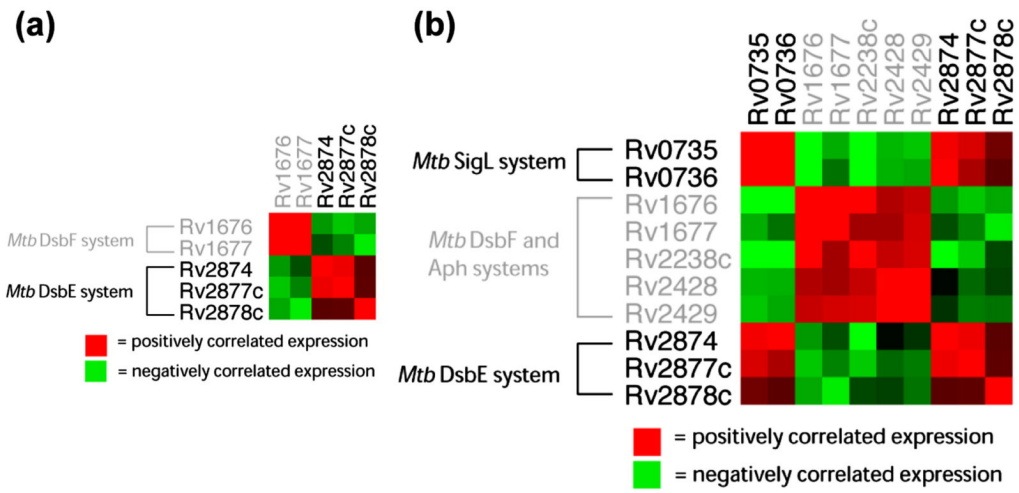

Figure 4.

Gene expression analysis. In figures 4a and 4b, red represents positive expression correlation and green represents negative correlation. The colors are shaded as to the degree of correlation, black indicates neither positive or negative correlation. Figure 4a contains the genes that encode for Rv1677 and its interaction partner Rv1676, as well as Rv2878c (*Mtb* DsbE) and its potential protein partners Rv2874 (DipZ, DsbD) and Rv2877c. Note *Mtb* DsbE (Rv2878c) and *Mtb* DsbF (Rv1677) and their respective protein partners have anticorrelated expression profiles. Figure 4b observes the correlated expression patterns of Rv1676, Rv1677, Rv2874, Rv2877c and Rv2878c in addition to AphC and sigma factor L systems; Rv2428 (AphC), Rv2429 (AphD) and Rv2238c (AphE), Rv0735 (SigL) and Rv0736 (anti-SigL). Note that *Mtb* DsbF and Aph systems have positive correlated expression patterns, which have anticorrelated expression patterns with *Mtb* DsbE and SigL systems (which have positively correlated expression to each other).

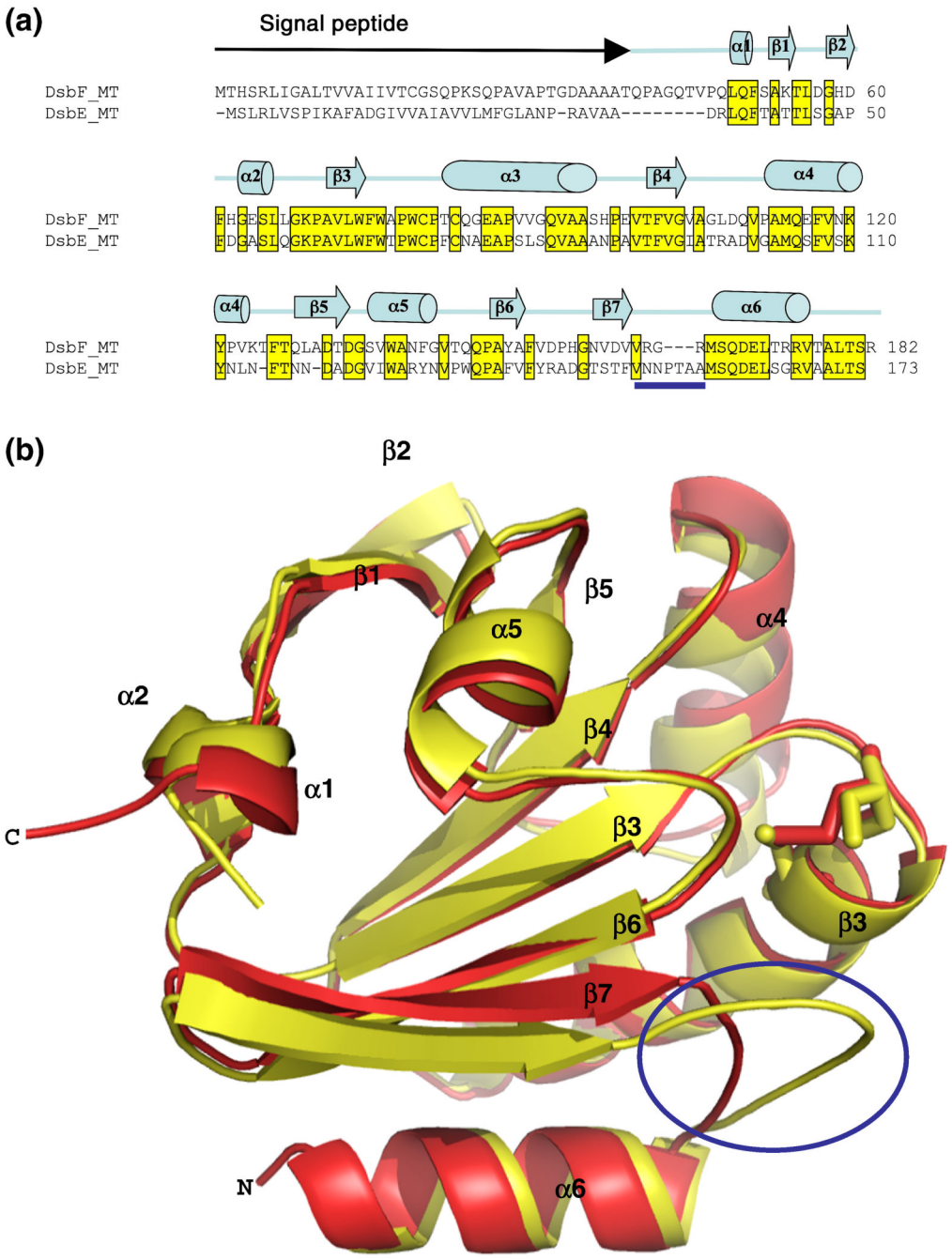

Figure 5.

Overall sequence and structural comparison of *Mtb* DsbF and *Mtb* DsbE. (a) Sequence alignment between *Mtb* DsbE and DsbF. The signal peptides for *Mtb* DsbE (Rv2878c) and *Mtb* DsbF (Rv1677) are depicted on the top line as a black arrow. The sequences are 54% identical and these residues are boxed in yellow. Residues underlined with the blue bar correspond to the loop region between β7 and α6. Secondary structure elements are depicted on the top line. (b) Superimposition of the structures of *Mtb* DsbF (red) and *Mtb* DsbE (yellow) which are shown as ribbon diagrams. The active-site cysteines are shown in sticks with the same respective coloring schemes: *Mtb* DsbF active-site oxidized cysteines, Cys81 and Cys84, are shown as red sticks and *Mtb* DsbE active-site reduced cysteines, Cys36 and Cys39, are

shown in yellow sticks. The most prominent difference between the two structures is the loop region between β7 and α6, (circled). In the *Mtb* DsbE structure (yellow) the loop is longer and appears to protect the active-site CxxC motif from solvent accessibility, whereas in the *Mtb* DsbF structure (red) this loop is shorter which allows greater accessibility to its active-site.

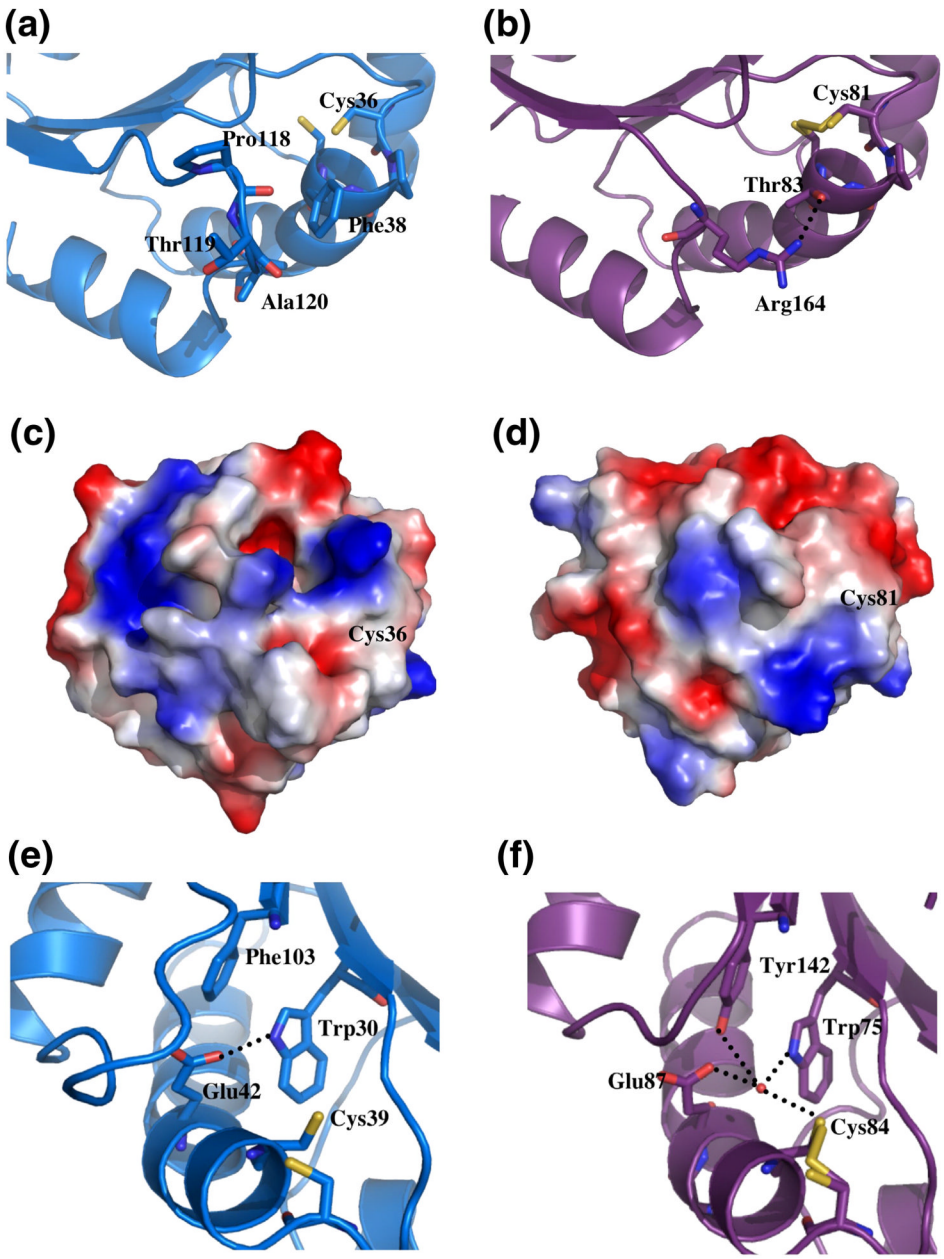

Figure 6.

Loop region, molecular surface representation and active-site comparisons of *Mtb* DsbF and *Mtb* DsbE. In (a), (b), (e) and (f) *Mtb* DsbE and *Mtb* DsbF are shown as ribbon diagrams in blue and purple, respectively. Stick models represent the pertinent amino acid residues where nitrogen, oxygen and sulfurs atoms are shown in blue, red and yellow, respectively. Hydrogen bonding is depicted with broken black lines. The images were generated in PYMOL. (a) The extended loop region in *Mtb* DsbE forms a cleft through a hydrophobic interaction with Phe38, which results in a more concave architecture surrounding the active-site. (b) The shorter loop region in *Mtb* DsbF stabilizes the active-site loop by a hydrogen bond between Arg164 and Thr83. Electrostatic molecular surface representation of (c) *Mtb* DsbE and (d) *Mtb* DsbF with the solvent-exposed active-site cysteines indicated. The overall position is equivalent to the active-sites shown in (a) and (b). Positive and negative electrostatic potentials are shown in

blue and red, respectively generated in PYMOL. The figure shows that *Mtb* DsbE has active-site is more solvent protected than *Mtb* DsbF. Also the surface surrounding the active-site of *Mtb* DsbF is more positively charged than that of *Mtb* DsbE. (e) and (f) show the conserved amino acid (Glu-Trp) pair in *Mtb* DsbE and *Mtb* DsbF, respectively. The hydrogen bond between Trp30 and Glu42 in the *Mtb* DsbE structure maintains a conformation in which the active-site residues are in their reduced form. Whereas, there is an extensive hydrogen bonding network between the amino acid pair (Trp75 and Glu87) and Tyr142, and which acts upon the active-site Cys81 facilitated by a water molecular in *Mtb* DsbF.

Table 1

X-ray diffraction data collection and atomic refinement for Rv1677 in its double conformation of its oxidized and reduced forms from *M. tuberculosis*

Space group	$P4_22_12$
Unit cell dimensions (Å)	100.12 × 100.12 × 30.09
pH of crystallization condition	7.0
Model includes residues	47–177
Data set	
Wavelength (Å)	1.00
Resolution range (Å)	90–1.6
Unique reflections (total)	23,073 (229,537)
Completeness (%)	100 (100)
R_{merge} [a]	6.8 (59.7)
I/σ	40.68 (3.85)
Model refinement	
Resolution range (Å)	10–1.6
No. of reflections (working/free)	16,851/1799
No. of protein atoms	1046
No. of water molecules	109
R_{work}/R_{free} [b] (%)	14.4/20.0 (25.1/33.5)
RMSD	
Bond lengths (Å)	0.012
Bond angles (°)	1.3
Ramachandran plot (%)	
Most favorable region	93.7
Additional allowed region	6.3
Disallowed region	0
PDB ID	3IOS

Statistics for the highest-resolution shell are given in parentheses.

[a] $R_{merge} = \Sigma|I-\langle I\rangle|/\Sigma I$.

[b] $R_{work} = \Sigma|F_{obs}-F_{calc}|/\Sigma F_{obs}$. R_{free} was computed identically except where all reflections belong to a test set of 5% randomly selected data.